Facial Synthesis, Stability, and Interaction of Ti$_3$C$_2$T$_x$@PC Composites for High-Performance Biocathode Microbial Electrosynthesis Systems

Ahsan Riaz Khan,[#] Weiming Wang,[#] Adnan Raza Altaf, Shumaila Shaukat, Hai-Jun Zhang,* Ata Ur Rehman, Zhang Jun, and Luogen Peng*

Read Online

ACCESS | Metrics & More | Article Recommendations | SI Supporting Information

ABSTRACT: Developing high-performance biocathodes remain one of the most challenging aspects of the microbial electrosynthesis (MES) system and the primary factor limiting its output. Herein, a hollow porous carbon (PC) fabricated with MXenes coated over an electrode was developed for MES systems to facilitate the direct delivery of CO$_2$ to microorganisms colonized. The result highlighted that MXene@PC (Ti$_3$C$_2$T$_x$@PC) has a surface area of 434 m^2/g. The Ti$_3$C$_2$T$_x$@PC MES cycle shows that in cycle 4 and cycle 5, the values are −309.2 and −352.3. Cyclic voltammetry showed that the coated electrode current response (mA) increased from −4.5 to −20.2. The substantial redox peaks of Ti$_3$C$_2$T$_x$@PC biofilms are displayed at −741, −516, and −427 mV vs Ag/AgCl, suggesting an enhanced electron transfer owing to the Ti$_3$C$_2$T$_x$@PC complex coating. Additionally, more active sites enhanced mass transfer and microbial development, resulting in a 46% rise in butyrate compared to the uncoated control. These findings demonstrate the value of PC modification as a method for MES-based product selection.
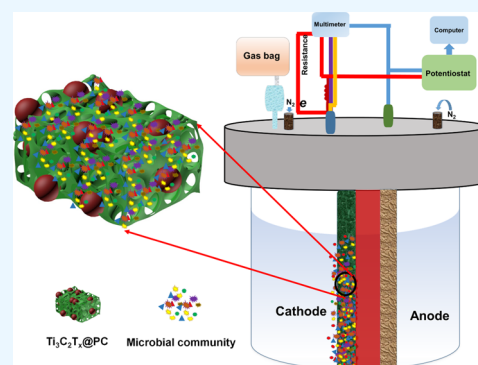
1. INTRODUCTION

Renewable energy-based alternative policies must be implemented due to exhaustive consumption of fossil fuels and high energy demand.[1−5] The modernism of well-organized technology for turning greenhouse gases like carbon dioxide (CO$_2$) into highly valued products will profoundly influence the environment and the economy.[6−9] Furthermore, carbon capture and utilization technologies are becoming more popular as the decarbonization of industries and circular economy become global concerns.[10−15] The bioelectrochemical process of microbial electrosynthesis (MES) can potentially convert CO$_2$ into a variety of short-chain carboxylic acids, alcohols, and methane, most of which are currently created from fossil-based precursors.[16−19] It is imperative to build inexpensive modified electrode materials because they are critical for selective microbial richness and serve as sites for microbial attachment and growth.[20−24]

Furthermore, the interaction between microbes and electrodes significantly affects MES production rates and efficiency. However, slow production rates are one of the major challenges to MES maturity, especially when combined with low current densities.[20,21,25,26] Additionally, a close microbe cathode interaction enables a local uptake of the reducing equivalents required for CO$_2$ reduction.[18,26] Furthermore, most electrodes have identified acetate as the primary MES product with additional compounds emerging in lesser quantities.[26] The lack of acetate expenditure has caused an

additional spotlight to be placed on product selectivity with better economic value. Black carbon derived from biomass (biochar) is a viable solution in this situation.[26] The production of electrodes may need less energy and produce less carbon dioxide if biochar is used. Additionally, PC may also encourage the co-selection of genes for antibiotic resistance, leading to the development of microbial communities that are both more resistant and selective.[27−30] Though, virgin biomass-derived porous carbon showed less electrical conductivity, especially when synthesized under low pyrolytic conditions.[31−33] Therefore, PC must be altered with an appropriate substance to enhance its bio-electrochemical functionality for MES implementation.
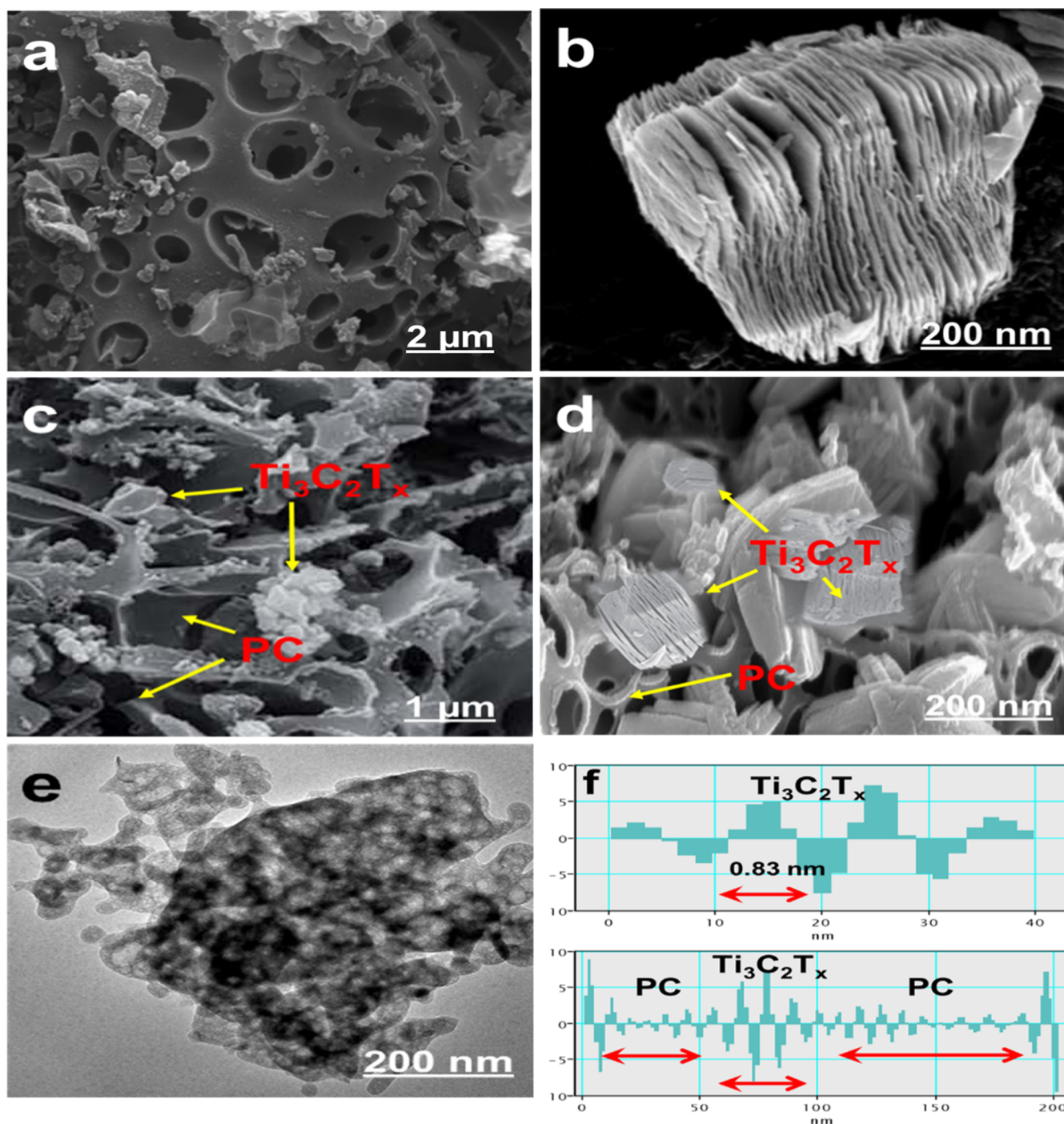
Multiple approaches for electrode modification have been suggested, such as fabricating the surface layer by adding nanowires or nanoparticles, graphene, and encapsulating the electrode with compounds that improve performance.[20,34−37] MXene (Ti$_3$C$_2$T$_x$), a recently discovered family of 2D materials, is a promising candidate for cathode coating due

Figure 1. SEM image of (a) PC, (b) $Ti_3C_2T_x$, and (c,d) $Ti_3C_2T_x$@PC composite and TEM image of (e) $Ti_3C_2T_x$@PC composite and (f) phase profile of $Ti_3C_2T_x$ and $Ti_3C_2T_x$@PC composite.

to its beneficial properties, such as superior conductivity, ion intercalation behavior, and hydrophilicity.[38−40] In addition to electrical conductivity, MXenes' remarkable pseudocapacitive properties are anticipated to enhance the performance of bio-electrochemical systems.[38,41] Furthermore, MXene sheets' interlayer space may support a greater bacterial load, triggering an improvement in biofilm formation. Second, it is suggested that MXenes can enhance the selective enrichment of microorganisms.[37,42,43] MXenes have been effectively implemented in pseudocapacitive high-capacity electrodes and supercapacitors.

Based on its high scientific surface area, structural adaptability, high electrical conductivity, exceptional chemical stability, and inexpensive price, biomass-derived carbon has recently attracted much interest as an electrode material for electrochemical devices. Currently, a variety of biomass resources, including sawdust, tea leaves, walnut shells, sunflower stalks, and many others, are used to produce biomass-derived carbon. These bio-based carbon distinctive porous network structures and higher electrical conductivity boost the capture and flow of electrons from the outer circuit and speed up the redox pair. Thus, combining MXenes with bio-based carbon to obtain hybrid materials is an effective

strategy to achieve high-performance bio-electrochemical functionality for MES implementation.

In this study, we investigate a new MXene-based composite ($Ti_3C_2T_x$@PC) coated over an electrode for the MES system for selective microorganism enrichment and product generation. In addition, constructing a low-cost technique to manufacture three-dimensional nanohybrids using aloe vera peel-derived porous carbon (PC). Two distinct MES electrode systems were used for the reduction of bicarbonate to various volatile fatty acids (VFA) subsequently, one with uncoated PC and the other with an MXene coating.[44] A diversified microbial inoculum was chosen based on its ability to generate a higher production rate/biomass over pure stains. In addition, a microbial study was carried out to pinpoint critical and relatively abundant microorganisms that were enriched due to MXene coating. As a result, this research aims to construct a hybrid MXene/PC biocathode with highly suitable morphologies for selective microbial enrichment and product generation in microbial electrosynthesis technologies. To the best of our knowledge, these novel hybrid materials have not been previously utilized as biocathode materials for MES.

2. RESULTS AND DISCUSSION

2.1. Characterization. Different characterization approaches were used to examine the uncoated, and $Ti_3C_2T_x$@PC-coated electrodes to show their potential physiochemical characteristics for MES applications. Scanning electron microscopy (SEM) and transmission electron microscopy (TEM) were used to analyze the electrode structural properties and morphologies at various magnifications (Figure 1). It should be emphasized that electrode surface characteristics substantially impact MES performance, biofilm development, and microbial proliferation. Figure 1a shows the final porous structure of PC, where it is clearly observed that the PC contains randomly oriented 3D pores throughout the structure. This irregular arrangement of pores causes the formation of a chain of active sites for diffusion of electrons through the CE material from the external circuit and improves microbial adhesion. On the other side, Figure 1b shows MXene-bordered structures with an open layer. These sheet-by-sheet structures further improve microbial adhesion by providing extra-large surface area and interlayer gaps. Figure 1c,d shows $Ti_3C_2T_x$@PC composite images at various scanning scales. In these images, the surface of PC and $Ti_3C_2T_x$-coated electrodes show a rough structure, where the advantage of $Ti_3C_2T_x$@PC composites has a large number of pores due to porous carbon and MXene-multilayered structures and in-between gaps. Figure 2e shows the TEM image of both $Ti_3C_2T_x$@PC and demonstrates the MXene is uniformly distributed across the PC materials. Figure 1f shows phase profiles of $Ti_3C_2T_x$ and $Ti_3C_2T_x$@PC composites based on Figure 1e, TEM images, and highlighted that the MXene and PC composite established a layer-after-layer structure and both materials have enough interlayer space for microbial activity. Therefore, $Ti_3C_2T_x$@PC materials help retain water content and provide enough space to facilitate substrate diffusion, nutrient accessibility to microbial cells, and microbial growth leading to biocathode enrichment over uncoated electrodes.

The X-ray diffraction (XRD) patterns of pure PC, $Ti_3C_2T_x$, and fabricated $Ti_3C_2T_x$@PC composites are shown in Figure 2.[39,45] The composite XRD study showed all of the MXene and PC distinctive peaks. In the composite, the highlighted 002 peak at 5° and 004 peak at 18° were corresponding for the
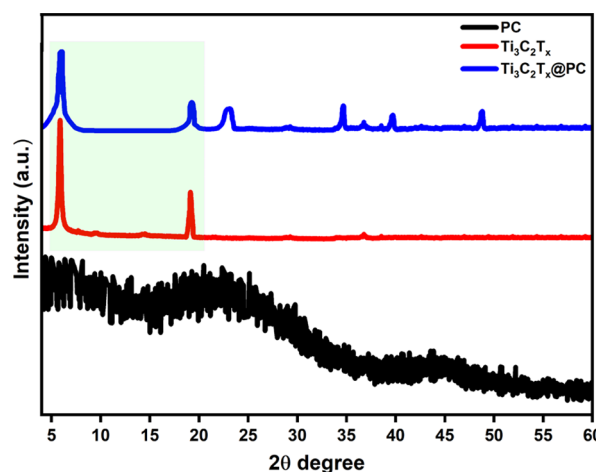

**Figure 2.** XRD pattern for $Ti_3C_2T_x$, PC, and $Ti_3C_2T_x$@PC composites.

successful incorporation of MXenes in the composite, and broadened peaks at 22, 35, 39, and 48° were attributable to PC. All the peaks of PC and $Ti_3C_2T_x$ are highly visible and show no other entity generated during the composite preparation process and indicate a successful composite preparation. A Brunauer−Emmett−Teller (BET) study was carried out to assess the surface area and pore size distribution. The study showed that N_2 adsorption/desorption isotherms indicate scientific surface areas of MXene and $Ti_3C_2T_x$@PC composites, as shown in Figure 3a. The adsorption capacity of MXenes significantly increases at low relative pressures ($p/p^o > 0.2$), indicating the presence of pores with even sizes throughout the samples. On the other hand, $Ti_3C_2T_x$@PC exhibit high adsorption capacities at low relative pressures ($p/p^o < 0.2$). Moreover, the surface areas of MXenes and $Ti_3C_2T_x$@PC were 389.4 and 434 m^2/g. Therefore, it is concluded from the BET studies that adsorption capacity and surface areas of $Ti_3C_2T_x$@PC show higher than that of MXenes. The advantage of as-prepared composite larger surfaces facilitates physiochemical properties and provides substrate diffusion, nutrient accessibility to microbial cells, and microbial growth leading to biocathode enrichment over uncoated electrodes.[27]

To understand the elemental composition of MXenes and $Ti_3C_2T_x$@PC composites, an X-ray photoelectron spectroscopy (XPS) study was conducted, and it is shown in Figure 3b. The distinctive Ti peaks in MXenes were identified to occur at 455.1, 455.7 eV (Ti−C 2p$_{3/2}$), and 461.4 eV (Ti−C 2p$_{1/2}$), while the characteristic C peak was revealed to occur at 284.5 eV C−C.[46] On the other hand, the composite shows MXene characteristic peaks and as well as Mn, Ca, K, and Mg peaks were observed at 638.89, 346.7, 294.6, and 88.7 eV, respectively.[47] It is also worth mentioning here that there are other functional groups (T_x) in the composite and serve as active sites that facilitate the binding of MXenes onto the substrate surface.

2.2. Current Density Evaluation. The MES cathodes were kept at a constant voltage of 800 mV (vs Ag/AgCl) to determine the current density.[48] In our MES setup, we used a pre-mixed microbial culture and growing media in a batch mode (see the Supporting Information). $Ti_3C_2T_x$@PC's output current density recovered after 22 h during the first cycle, demonstrating fast microbial adsorption.
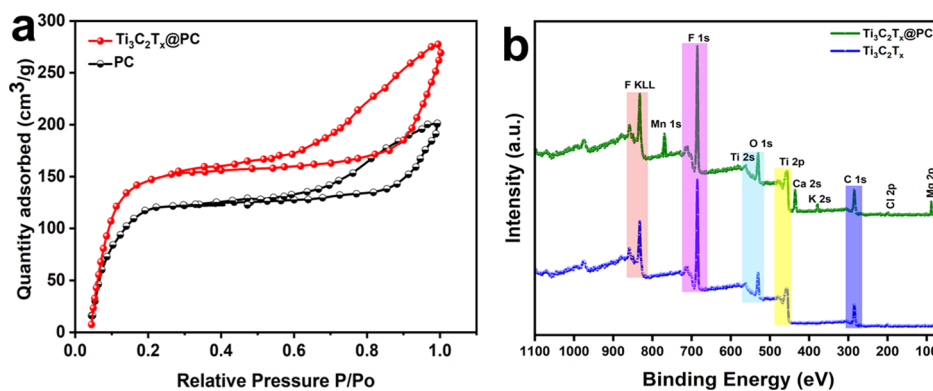
Figure 3. (a) Brunauer−Emmett−Teller (BET) adsorption−desorption isotherm of PC and composite and (b) X-ray photoelectron spectroscopy (XPS) spectrum of $Ti_3C_2T_x$ and $Ti_3C_2T_x$@PC.
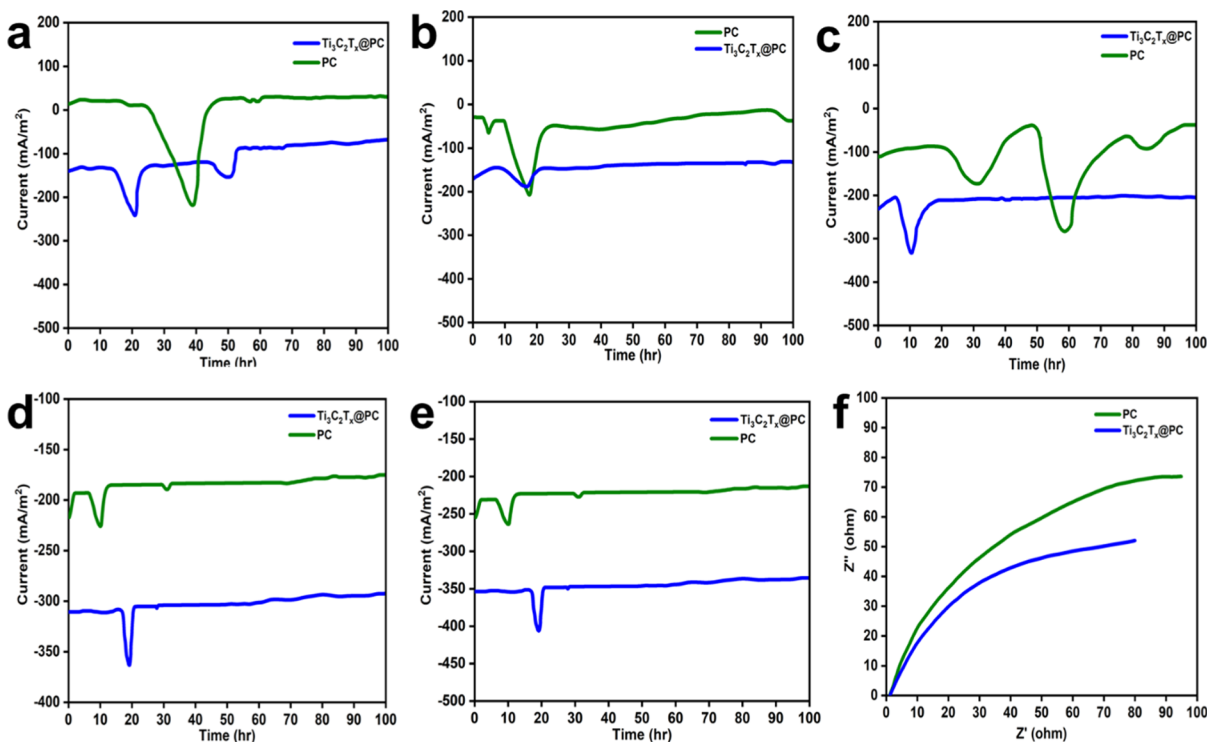

Figure 4. (a) Current density performance using uncoated PC and $Ti_3C_2T_x$@PC cathodes at an applied voltage of −0.8 V for MES cycles (a) 1, (b) 2, (c) 3, (d) 4, (e) 5, and (f) Nyquist curve for uncoated PC and $Ti_3C_2T_x$@PC electrodes.

Both coated and uncoated PC exhibit an increase in their current density efficiency, indicating a rise in the current density output, as shown in Figure 4b−e. The estimated average density (mA m^{-2}) was calculated for each MES cycle. At the end of cycle 2 (Figure 4b), the average current density increased from −58.3 (PC) to −140.6 ($Ti_3C_2T_x$@PC) and at the end of cycle 3 from −106.6 (porous carbon) to −221.2 ($Ti_3C_2T_x$@PC) (Figure 4c). While for cycle 4 and cycle 5, the value was −187.1 and −225.4 for PC and −309.2 and −352.3 for $Ti_3C_2T_x$@PC, respectively. A 2.1- and 2.5-fold increase in current density output was recorded in cycles 4 and 5, highlighting a significant MES performance enhancement (Figure 4d,e). In line with these findings, MXenes may also improve the efficacy of systems and biological catalytic redox reactions. This enhanced bio-electrochemical performance may be attributable to a decrease in electrode charge-transfer resistance (R_{ct}), as determined by Nyquist curves and electrochemical impedance spectroscopy (EIS) analysis

(Figure 4f). Furthermore, the Coulomb efficiency (CE) was also evaluated for all MES cycles and average 24 and 18% CEs were observed for $Ti_3C_2T_x$@PC and PC, respectively, as shown in Figure 5. The R_{ct} at the electrolyte−cathode interface was determined to be lower for the $Ti_3C_2T_x$@PC (108 Ω) electrode as compared to an uncoated electrode (137 Ω) based on these observations. This decline in R_{ct} indicates that the MXene coating improved the electrode charge transfer, hence enhancing the current density and MES performance. The current density performance between the cathode and the microbes was boosted as a result of the decrease in R_{ct}. From this, we can infer that PC exo−electrogenic activity, which aids direct and indirect electron transfer, may be responsible for its enhanced performance.

2.3. Cyclic Voltammetry and Electrochemical Impedance Spectroscopy Analysis. The electrocatalytic activity of each CE is studied by performing cyclic voltammogram (CV) scans using the three-electrode setup, as depicted in
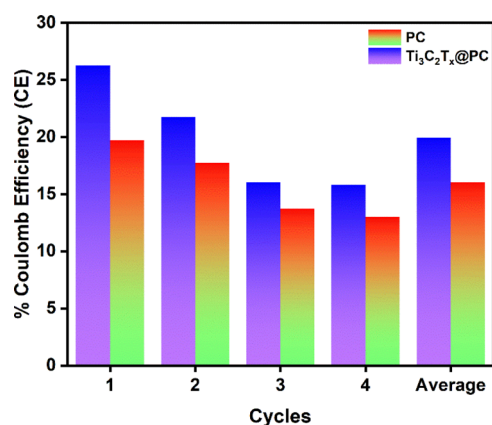
Figure 5. % CE for MES cycles using PC and Ti$_3$C$_2$T$_x$@PC biocathodes.

Figure 6. The capacitive properties of a material were shown by the CV closed area size, which was larger for the coated electrode systems than the uncoated electrode. The role of MXenes on an electron uptake was investigated using CV at several scan rates ranging from 5 to 200 mV/s. The results showed that the current response (mA) increased for the coated electrode from −4.5 (Figure 6a) to −20.2 (Figure 6b), showing improved electron-transfer behavior. It is suggested that this change is probably due to MXenes greater conductivity and electrogenesis capabilities. This increased

effectiveness could be related to the synergistic interaction between PC and MXenes, which has stronger conductivity and capacitive behavior for electrogenesis. These findings are consistent with the idea that improved electrode capacitance can facilitate electron transmission by decreasing charge-transfer resistance, which agrees with the above results.

This was done in order to determine the electron uptake by the microbes. The PC material had a couple of redox peaks, although both the size and intensity of the peaks were less pronounced in comparison to those showed by the Ti$_3$C$_2$T$_x$@PC biocathode, as presented in Figure 6c. This suggested that the biofilm in all coated electrode systems had improved electrochemical activity.

The substantial redox peaks of Ti$_3$C$_2$T$_x$@PC biofilm are displayed at −741, −516, and −427 mV vs Ag/AgCl, suggesting an enhanced electron transfer owing to the Ti$_3$C$_2$T$_x$@PC complex coating. The diversity of the experimental settings, the electrode substance, and the enrichment of free or biofilm-bound catalysts could influence the difference in the measured redox values. It is suggested that these changes are associated with either single or mixed microbial inoculum in the study.

2.4. Microbial Electrosynthesis of VFA. At greater concentrations, HPLC was used to detect the formation of volatile fatty acids (FFAs), including butyric acid. On the other hand, the amounts of acetic acid and propionic acid were found to be significantly lower. A larger quantity of butyrate
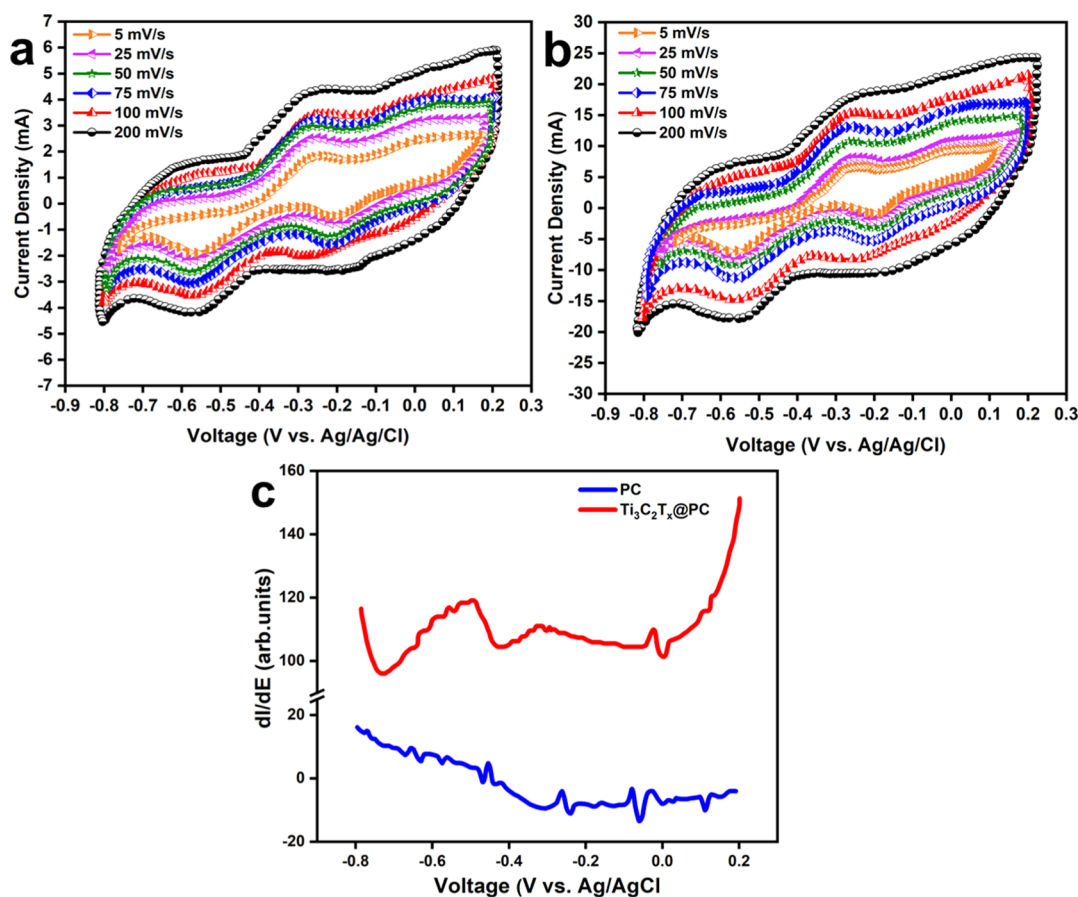
Figure 6. CV profiles recorded at different scan rates (5−75 mV/s) and applied potential (−0.8 to +0.2 V) for (a) PC, (b) Ti$_3$C$_2$Tx@PC, and (c) first derivative deduced from the CV (from positive to negative voltage) recorded using uncoated PC and MXene@PC electrodes. By exploring the first CV derivative presented in Figure 6c, the biofilm on both electrodes was assessed to further study the electrochemical activity.
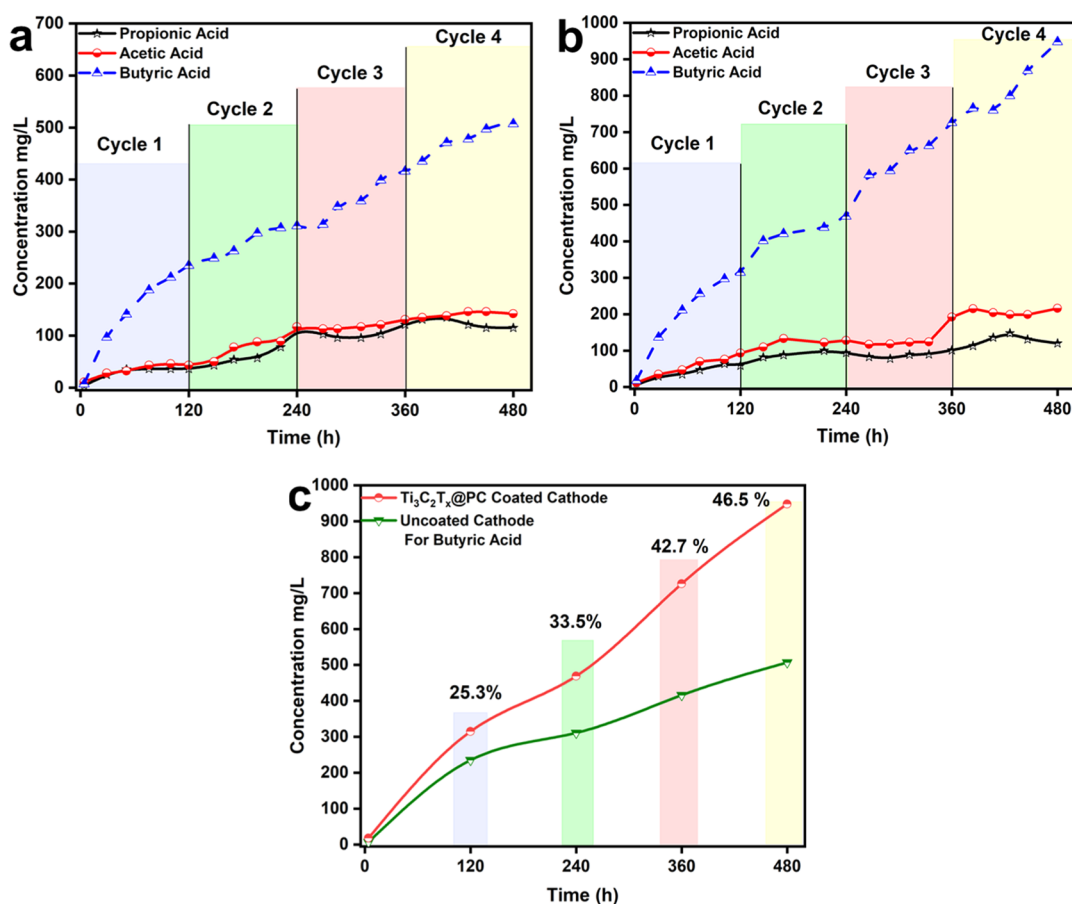
Figure 7. Accumulated concentration profile of VFAs (butyrate, acetate, and propionate) using the (a) uncoated PC cathode, (b) Ti$_3$C$_2$T$_x$@PC cathode, and (c) butyric acid comparative profile for coated and uncoated PCs.

was produced as a consequence of the PC ability to impede the growth of specific microorganisms, which in turn promoted selective microbial enrichment. However, acetic and propionic acids were generated in lower titers. On the other hand, Ti$_3$C$_2$T$_x$@PC composites inhibit larger growth than PC for certain microbes and alternately highly promote selective microbial enrichment for higher butyrate concentrations while acetic and propionic acids are generated in lower titers. Porous carbon volatile organic compounds and pyrolysis products are known to promote and inhibit the growth of various microbes; therefore, this finding makes intuitive sense.

This strategy encourages the pro-selection of genes for selective microbial enrichment and antibiotic resistance, which increases butyrate concentrations. However, for MES cycles 1, 2, 3, and 4, the MXene-coated biocathode revealed enhanced butyrate synthesis with 25, 33, 42, and 46% higher than the uncoated PC, respectively (Figure 7). This indicates that MXene tends to change the composition of microbial populations, loading them with more microorganisms that produce butyrate as their principal product. In addition, the richness and co-existence of various acetogenic and fermentative microbes suggests that butyrate formation may occur via multiple pathways. The bioconversion of acetate to butyrate may occur via the reductive acetylCoA or Wood-Ljungdahl pathway. Acetate is digested more quickly than butyrate, and some anaerobic microbes can effectively utilize acetate. In addition, the Ti$_3$C$_2$T$_x$@PC composite possesses larger number sheets by sheet structure, which strongly facilitates the nutrient uptake by microbial cells. Additionally, essential nutrients, such

as magnesium, salt, nitrogen, potassium, and phosphorus, may promote microorganism growth and biofilm formation. The profitability of MES systems employing various common and modified cathode materials was compared to that of Ti$_3$C$_2$T$_x$@PC composites both coated and uncoated cathode materials (Table S1). Strategic factors, such as cathode composition, applied potential, and microbial inoculum enrichment, may be responsible for MES performance differences, including current density, VFA products, and yields. Several studies have found a correlation between improved MES performance and upgraded cathode properties. These findings are in agreement with better electrochemical properties of Ti$_3$C$_2$T$_x$@PC, which indicates that high electron uptake by the microbial catalyst is critical for greater VFA formation. This proved that adding MXene to PC (PC) modifies the contact, increasing microbial production. Therefore, the high current density performance of Ti$_3$C$_2$T$_x$@PC composite as an anode showed effective results for MES systems.

3. CONCLUSIONS

In summary, we proposed a hybrid MXene@PC composite (Ti$_3$C$_2$T$_x$/PC) coated over an electrode for butyrate production as the primary MES product. The proposed electrode retains the advantages of 2D materials and porous carbon by decreasing the electrode resistance to support and increase in a capacitive behavior. The main results are the following:
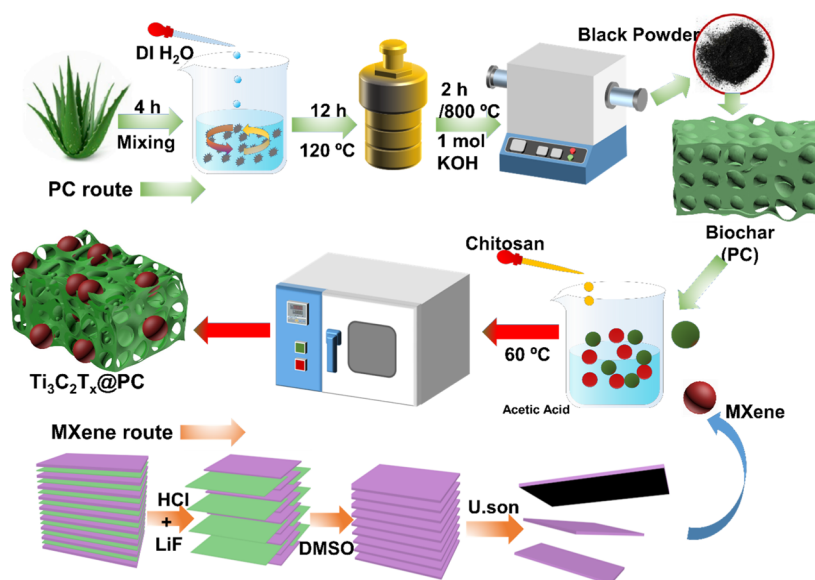
Figure 8. Schematic diagram of Ti$_3$C$_2$T$_x$@PC using porous carbon synthesis (PC route), MXene synthesis (MXene route), and composite preparation.

(1) the average current density for cycle 4 and cycle 5, the values were −187.1 and −225.4 for PC and −309.2 and −352.3 for Ti$_3$C$_2$T$_x$@PC, respectively, which means that 2.1- and 2.5-fold increase in current density output was recorded in cycles 4 and 5, which showed a significant improvement in the MES performance.

(2) Due to MXene's greater conductivity and electrogenesis capabilities, the current response (mA) increased for the coated electrode from −4.5 to −20.2, showing improved electron-transfer behavior.

(3) The substantial redox peaks of Ti$_3$C$_2$T$_x$@PC biofilm are displayed at −741, −516, and −427 mV vs Ag/AgCl, suggesting an enhanced electron transfer owing to the Ti$_3$C$_2$T$_x$@PC complex coating.

(4) MES cycles 1, 2, 3, and 4, the MXene-coated biocathode revealed enhanced butyrate synthesis with 25, 33, 42, and 46% higher than the uncoated PC.

4. MATERIALS AND METHODOLOGY

4.1. Materials. Ti$_3$AlC$_2$ MAX phase powders (400 mesh) were purchased from 11 Technology Co., Ltd Beijing. LiF (98.5%) and HCl was bought from Fuchen Chemical Reagent Factory in Tianjin. Sigma-Aldrich provided dimethyl sulfoxide (DMSO).

4.2. Sample Preparations. *4.2.1. Synthesis of MXene.* Figure 8 (route MXene) describes a general map of MXene preparation from Ti$_3$AlC$_2$ phase powders. Around 1 g of LiF was added to 10 mL of 9 molar HCl (37% wt) and stirred for 15 mins at 35 °C. After that, chemically etched Al from Ti$_3$AlC$_2$ was done by adding 1 g of MAX gradually to the solution for the next 36 h at 35 °C in a water bath to produce HF. Now, the resultant suspension was washed with deionized water (DI H$_2$O) via centrifugation at 3500 rpm for 10 min per cycle until the pH of the supernatant reached approximately 6 and then, the sample was dried in a vacuum oven for the whole night at 80 °C. After that, 40 mL of DMSO was mixed and stirred for 18 h in the sediment to intercalate MXene sheets and again centrifuge to collect DMSO. The precipitate was then dispersed into water via an ultrasonication process for 1 h

with a frequency of 20 kHz (Power: 600 W). The obtained few-layered Ti$_3$C$_2$T$_x$ was centrifuged and washed with water and ethanol several times. The resulting material was used without further modification or processing. The concentration of the as-prepared MXene solution was approximately 1 mg/Ml.[49,50]

4.2.2. Synthesis of PC. Aloe vera peel-derived porous carbon nomenclature as porous carbon (PC) was extracted by drying aloe vera peel waste at 105 °C, as presented in Figure 8 (route PC). The homogenous mixture was obtained by stirring the dried biomass with deionized water for 4 h. Subsequently, the obtained slurry was transferred into a Teflon-lined stainless-steel autoclave and treated hydrothermally at 120 °C for 12 h. The obtained black powder was activated by 1 mol/L KOH then sintered at 800 °C for 2 h in a tubular furnace under a N$_2$ atmosphere. Then, the powder was washed with 1 mol/L HCl, deionized water, and absolute ethanol and finally dried to obtain PC.[51]

4.2.3. Synthesis of MXene@PC Electrode (Ti$_3$C$_2$T$_x$@PC) Preparation. After cooling, a 10 g chunk of aloe vera peel-derived porous carbon was dipped in a solution of chitosan (1 g) and Ti$_3$C$_2$T$_x$ (25 mg) dispersed in C$_2$H$_4$O$_2$ (2%) and stirred for 30 mins, as presented in Figure 9. The resultant biomass monolith was enclosed in a stainless-steel mesh, and washed with deionized water at vacuum dried at 60 °C. The prepared electrode had a surface area of 5 × 5 cm^2 and a thickness of 1 cm, respectively. The MXene coating procedure was simple to use and did not require an intense experimental setup, making it a practical and environmentally friendly approach. The same steps were used to prepare the uncoated PC electrode except for adding MXenes.

4.2.4. Characterization. The morphological study of MXene and Ti$_3$C$_2$T$_x$@PC composite was characterized through TEM (Tecnai G^2 F20 S-TWIN) and SEM. TEM samples were prepared by scratching the SnO$_2$/MXene powder off Cu-foil and dispersing it in ethanol. SEM samples were gold-sputtered before the observation. Pore size distributions of MXene and MgSO$_4$/MXene were calculated by the BJH method from the desorption isotherm and surface areas were calculated by the BET method at 77 K. The physicochemical
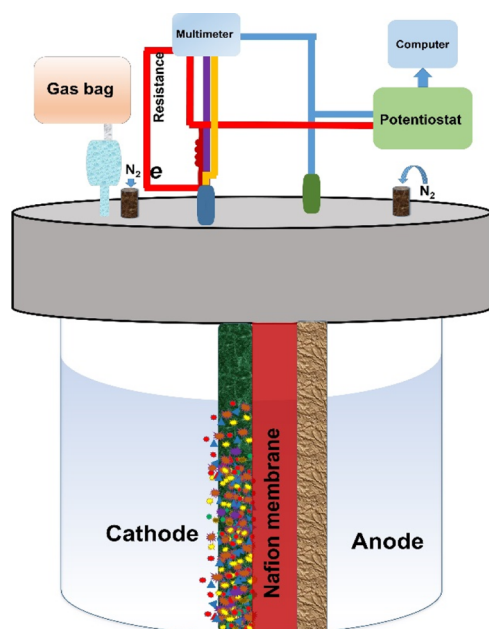
Figure 9. Schematic diagram of MXene@PC electrode preparation and MES operation.

measurement of samples was investigated at Rigaku Smart Lab II powder X-ray diffraction (Rigaku Co., Tokyo, Japan) using an average Cu Kα1 + Kα2 radiation (λ = 0.15425 A) source. XPS characterized the binding energy of samples using a scanning X-ray micrograph (ULVAC-PHI II; Quantera, Tokyo, Japan.

4.2.5. MES System Construction and Operation. As the MES assembly, a dual plexiglass tank with a 0.2 L (anode/cathode) capacity and dimensions of 5 cm × 5 cm × 8 cm was used. Carbon fabric infused with 20 wt % Pt was utilized as the anode and cathode materials, which was Ti$_3$C$_2$T$_x$@PC. Both anode/cathode chambers were separated by a Nafion 117 proton exchange membrane (DuPont Co.; Wilmington, DE, USA) pretreated with H$_2$O$_2$ (3%) and H$_2$SO$_4$ (0.5 M). A gas bag containing N$_2$ was used to constantly purge both the anode and cathode chamber. Both MES modules were autoclaved prior installation to assure system decontamination. The efficiency of the MES was assessed throughout four cycle periods, every one of which operated for 120 h at a stable cathodic potential of about −800 mV (vs AgCl). At the beginning of each cycle, new growth media containing bicarbonate as a carbon source was added. Sodium bromoethanesulfonate was employed to prevent the growth of additional methanogens and the synthesis of methane during the microbial enrichment phase. The Supporting Information contains comprehensive information on the MES culture, selective enrichment, and growing media. A magnetic stirrer (180 rpm) ensures that the biological catholyte was homogeneously mixed, whereas a temperature controller maintains the system temperature at 35 ± 1 °C.[26]

4.2.6. Electrochemical Measurements. A multi-channel potentiostat with a three-electrode system was used. The Ti$_3$C$_2$T$_x$@PC composite and uncoated PC were designated as working electrodes, while the anode served as a counter electrode. The biocathode was evaluated using CV and chronoamperometry (CA) and analysis using EIS. At a constant cathodic potential (−800 mV vs Ag/AgCl), the current−time behavior was studied using CA. Three cycles of

CV analysis were performed to evaluate electrochemical properties at various scan rates (5−200 mV/s). The electrode and electrolyte were kept in balance by putting fresh growth medium in the cathode compartment 24 h before the CV analysis. The electrolyte for EIS was a potassium ferricyanide (5 mM) and phosphate-buffered (5 mM) solution. MXene@ PC and PC EIS analyses were performed at a frequency range from 100 kHz to 0.01 Hz. The EIS study was performed over a large frequency spectrum (100 kHz−0.01 Hz) utilizing a constant cathodic potential (+200 mV vs AgCl) and a Pt wire as the counter electrode (CE).[20]

■ ASSOCIATED CONTENT

Ⓢ Supporting Information

The Supporting Information is available free of charge at https://pubs.acs.org/doi/10.1021/acsomega.2c08163.

> Supporting information file contains, microbial culture/ sludge, media and culture conditions, and microbial community analysis data (PDF)

■ AUTHOR INFORMATION

Corresponding Authors

Hai-Jun Zhang − *Department of Interventional and Vascular Surgery, Shanghai Tenth People's Hospital, Tongji University School of Medicine, Shanghai 200072, China; National United Engineering Laboratory for Biomedical Material Modification, Branden Industrial Park, Qihe Economic & Development Zone, Dezhou City, Shandong 251100, China;* Email: zhanghaijun@tongji.edu.cn

Luogen Peng − *The Affiliated Changsha Central Hospital, Department of Oncology, Hengyang Medical School, University of South China, Changsha 410008, China;* Email: 2022050054@usc.edu.cn

Authors

Ahsan Riaz Khan − *Department of Interventional and Vascular Surgery, Shanghai Tenth People's Hospital, Tongji University School of Medicine, Shanghai 200072, China; National United Engineering Laboratory for Biomedical Material Modification, Branden Industrial Park, Qihe Economic & Development Zone, Dezhou City, Shandong 251100, China*

Weiming Wang − *The Affiliated Changsha Central Hospital, Department of Oncology, Hengyang Medical School, University of South China, Changsha 410008, China*

Adnan Raza Altaf − *School of Engineering, Huazhong, Agricultural University, Wuhan 430070, China;* Ⓞ orcid.org/0000-0002-4723-2672

Shumaila Shaukat − *College of Chemistry and Materials Science, Northwest University, Xi'an 710069, China*

Ata Ur Rehman − *College of Chemistry and Materials Science, Northwest University, Xi'an 710069, China;* Ⓞ orcid.org/ 0000-0002-8227-5352

Zhang Jun − *Research Center for Translational Medicine, Shanghai East Hospital, School of Medicine, Tongji University, Shanghai 200092, China; Shanghai Institute of Stem Cell Research and Clinical Translation, Shanghai 200020, China*

Complete contact information is available at: https://pubs.acs.org/10.1021/acsomega.2c08163

Author Contributions

#A.R.K. and W.W. contributed equally to this work.

Notes

The authors declare no competing financial interest.

◼ REFERENCES

(1) Ur Rehman, A.; Maosheng, Z.; Hayat, A. Water sorption studies on ZnSO4-zeolite composite as potential thermochemical heat storage materials. *Int. J. Energy Res.* 2020, 44, 269−281.

(2) Ullah, A.; Khan, J.; Sohail, M.; Hayat, A.; Zhao, T. K.; Ullah, B.; Khan, M.; Uddin, I.; Ullah, S.; Ullah, R.; et al. Fabrication of polymer carbon nitride with organic monomer for effective photocatalytic hydrogen evolution. *J. Photochem. Photobiol., A* 2020, 401, 112764.

(3) Hayat, A.; Shaishta, N.; Mane, S. K. B.; Hayat, A.; Khan, J.; Rehman, A. U.; Li, T. Molecular engineering of polymeric carbon nitride based Donor-Acceptor conjugated copolymers for enhanced photocatalytic full water splitting. *J. Colloid Interface Sci.* 2020, 560, 743−754.

(4) Iqbal, M.; Karim, A.; Ali, S.; Bilal, H.; Rehman, A. U. Synthesis, Characterization, Structural Description, Micellization Behavior, DNA Binding Study and Antioxidant Activity of 4, 5 and 6-Coordinated Copper (II) and Zinc (II) Complexes. *Z. Anorg. Allg. Chem.* 2020, 646, 895−903.

(5) Liu, S.; Yin, Y.; Hui, K. S.; Hui, K. N.; Lee, S. C.; Jun, S. C. High-Performance Flexible Quasi-Solid-State Supercapacitors Realized by Molybdenum Dioxide@Nitrogen-Doped Carbon and Copper Cobalt Sulfide Tubular Nanostructures. *Adv. Sci.* 2018, 5, 1800733.

(6) Tainio, M.; Jovanovic Andersen, Z.; Nieuwenhuijsen, M. J.; Hu, L.; De Nazelle, A.; An, R.; Garcia, L. M.; Goenka, S.; Zapata-Diomedi, B.; Bull, F.; et al. Air pollution, physical activity and health: A mapping review of the evidence. *Environ. Int.* 2021, 147, 105954.

(7) Zhao, T.; Munis, A.; Rehman, A. U.; Zheng, M. Corrosion behavior of aluminum in molten hydrated salt phase change materials for thermal energy storage. *Mater. Res. Express* 2020, 7, 015529.

(8) Munis, A.; Zhao, T.; Zheng, M.; Rehman, A. U.; Wang, F. A newly synthesized green corrosion inhibitor imidazoline derivative for carbon steel in 7.5% NH4Cl solution. *Sustainable Chem. Pharm.* 2020, 16, 100258.

(9) Rehman, A. U.; Maosheng, Z.; Hayat, A. Hydration performance and cycling stability of three TCM: MgSO4, ZnSO4 and FeSO4. *Int. J. Energy Res.* 2020, 44, 6981−6990.

(10) Khan, M.; Hayat, A.; Baburao Mane, S. K.; Li, T.; Shaishta, N.; Alei, D.; Zhao, T. K.; Ullah, A.; Zada, A.; Rehman, A.; et al. Functionalized nano diamond composites for photocatalytic hydrogen evolution and effective pollutant degradation. *Int. J. Hydrogen Energy* 2020, 45, 29070−29081.

(11) Nguyen, M. H.; Zbair, M.; Dutournié, P.; Gervasini, A.; Vaulot, C.; Bennici, S. Toward new low-temperature thermochemical heat storage materials: Investigation of hydration/dehydration behaviors of MgSO4/Hydroxyapatite composite. *Sol. Energy Mater. Sol. Cells* 2022, 240, 111696.

(12) Yoro, K. O.; Daramola, M. O. CO2 emission sources, greenhouse gases, and the global warming effect. In *Advances in Carbon Capture*; Elsevier, 2020; pp 3−28.

(13) Rehman, A. U.; Khan, M.; Maosheng, Z. Hydration behavior of MgSO4−ZnSO4 composites for long-term thermochemical heat storage application. *J. Energy Storage* 2019, 26, 101026.

(14) Liu, S.; Yin, Y.; Shen, Y.; Hui, K. S.; Chun, Y. T.; Kim, J. M.; Hui, K. N.; Zhang, L.; Jun, S. C. Phosphorus Regulated Cobalt Oxide@Nitrogen-Doped Carbon Nanowires for Flexible Quasi-Solid-State Supercapacitors. *Small* 2020, 16, 1906458.

(15) Ur Rehman, A.; Zhao, T.; Shah, M. Z.; Khan, Y.; Hayat, A.; Dang, C.; Zheng, M.; Yun, S. Nanoengineering of MgSO4 nanohybrid on MXene substrate for efficient thermochemical heat storage material. *Appl. Energy* 2023, 332, 120549.

(16) Vassilev, I.; Dessì, P.; Puig, S.; Kokko, M. Cathodic biofilms−A prerequisite for microbial electrosynthesis. *Bioresour. Technol.* 2022, 348, 126788.

(17) Bian, B.; Singh, Y.; Rabaey, K.; Saikaly, P. E. Nickel-Coated ceramic hollow fiber cathode for fast enrichment of chemo-lithoautotrophs and efficient reduction of CO2 in microbial electrosynthesis. *Chem. Eng. J.* 2022, 450, 138230.

(18) Wang, D.; Liang, Q.; Chu, N.; Zeng, R. J.; Jiang, Y. Deciphering mixotrophic microbial electrosynthesis with shifting product spectrum by genome-centric metagenomics. *Chem. Eng. J.* 2023, 451, 139010.

(19) Roy, M.; Aryal, N.; Zhang, Y.; Patil, S. A.; Pant, D. Technological progress and readiness level of microbial electrosynthesis and electrofermentation for carbon dioxide and organic wastes valorization. *Curr. Opin. Green Sustainable Chem.* 2022, 35, 100605.

(20) Tahir, K.; Miran, W.; Jang, J.; Maile, N.; Shahzad, A.; Moztahida, M.; Ghani, A. A.; Kim, B.; Jeon, H.; Lee, D. S. MXene-coated biochar as potential biocathode for improved microbial electrosynthesis system. *Sci. Total Environ.* 2021, 773, 145677.

(21) Li, S.; Kim, M.; Jae, J.; Jang, M.; Jeon, B.-H.; Kim, J. R. Solid neutral red/Nafion conductive layer on carbon felt electrode enhances acetate production from CO2 and energy efficiency in microbial electrosynthesis system. *Bioresour. Technol.* 2022, 363, 127983.

(22) Song, Y. E.; Mohamed, A.; Kim, C.; Kim, M.; Li, S.; Sundstrom, E.; Beyenal, H.; Kim, J. R. Biofilm matrix and artificial mediator for efficient electron transport in CO2 microbial electrosynthesis. *Chem. Eng. J.* 2022, 427, 131885.

(23) Liu, S.; Kang, L.; Henzie, J.; Zhang, J.; Ha, J.; Amin, M. A.; Hossain, M. S. A.; Jun, S. C.; Yamauchi, Y. Recent Advances and Perspectives of Battery-Type Anode Materials for Potassium Ion Storage. *ACS Nano* 2021, 15, 18931−18973.

(24) Rehman, A. U.; Zhao, T.; Muhammad, I.; Rasheed, S.; Shah, R.; Altaf, A. R.; Zhang, F.; Yun, S. MgCl2-MXene based nanohybrid composite for efficient thermochemical heat storage application. *J. Energy Storage* 2023, 59, 106509.

(25) Zhang, S.; Jiang, J.; Wang, H.; Li, F.; Hua, T.; Wang, W. A review of microbial electrosynthesis applied to carbon dioxide capture and conversion: The basic principles, electrode materials, and bioproducts. *J. CO2 Util.* 2021, 51, 101640.

(26) Tahir, K.; Maile, N.; Ghani, A. A.; Kim, B.; Jang, J.; Lee, D. S. Development of a three-dimensional macroporous sponge biocathode coated with carbon nanotube−MXene composite for high-performance microbial electrosynthesis systems. *Bioelectrochemistry* 2022, 146, 108140.

(27) Chu, N.; Hao, W.; Wu, Q.; Liang, Q.; Jiang, Y.; Liang, P.; Ren, Z. J.; Zeng, R. J. Microbial electrosynthesis for producing medium chain fatty acids. *Engineering* 2022, 16, 141−153.

(28) Chen, Q.; Lan, P.; Wu, M.; Lu, M.; Pan, B.; Xing, B. Biochar mitigates allelopathy through regulating allelochemical generation from plants and accumulation in soil. *Carbon Research* 2022, 1, 6.

(29) Altaf, A. R.; Adewuyi, Y. G.; Teng, H.; Liu, G.; Abid, F. Elemental mercury (Hg^0) removal from coal syngas using magnetic tea-biochar: Experimental and theoretical insights. *J. Environ. Sci.* 2022, 122, 150−161.

(30) Liu, A.; Liang, X.; Ren, X.; Guan, W.; Gao, M.; Yang, Y.; Yang, Q.; Gao, L.; Li, Y.; Ma, T. Recent progress in MXene-based materials: potential high-performance electrocatalysts. *Adv. Funct. Mater.* 2020, 30, 2003437.

(31) Altaf, A. R.; Teng, H.; Zheng, M.; Ashraf, I.; Arsalan, M.; Rehman, A. U.; Gang, L.; Pengjie, W.; Yongqiang, R.; Xiaoyu, L. One-step synthesis of renewable magnetic tea-biochar derived from waste tea leaves for the removal of Hg^0 from coal-syngas. *J. Environ. Chem. Eng.* 2021, 9, 105313.

(32) Selvam, S. M.; Paramasivan, B. Microwave assisted carbonization and activation of biochar for energy-environment nexus: A review. *Chemosphere* **2022**, *286*, 131631.

(33) You, S.; Li, W.; Zhang, W.; Lim, H.; Kua, H. W.; Park, Y.-K.; Igalavithana, A. D.; Ok, Y. S. Energy, economic, and environmental impacts of sustainable biochar systems in rural China. *Crit. Rev. Environ. Sci. Technol.* **2022**, *52*, 1063−1091.

(34) Rengasamy, K.; Ranaivoarisoa, T.; Bai, W.; Bose, A. Magnetite nanoparticle anchored graphene cathode enhances microbial electrosynthesis of polyhydroxybutyrate by Rhodopseudomonas palustris TIE-1. *Nanotechnology* **2020**, *32*, 035103.

(35) Thatikayala, D.; Min, B. Copper ferrite supported reduced graphene oxide as cathode materials to enhance microbial electrosynthesis of volatile fatty acids from CO_2. *Sci. Total Environ.* **2021**, *768*, 144477.

(36) Gao, Y.; Li, Z.; Cai, J.; Zhang, L.; Liang, Q.; Jiang, Y.; Zeng, R. J. Metal nanoparticles increased the lag period and shaped the microbial community in slurry-electrode microbial electrosynthesis. *Sci. Total Environ.* **2022**, *838*, 156008.

(37) Chen, H.; Simoska, O.; Lim, K.; Grattieri, M.; Yuan, M.; Dong, F.; Lee, Y. S.; Beaver, K.; Weliwatte, S.; Gaffney, E. M.; et al. Fundamentals, applications, and future directions of bioelectrocatalysis. *Chem. Rev.* **2020**, *120*, 12903−12993.

(38) Li, X.; Huang, Z.; Shuck, C. E.; Liang, G.; Gogotsi, Y.; Zhi, C. MXene chemistry, electrochemistry and energy storage applications. *Nat. Rev. Chem* **2022**, *6*, 389−404.

(39) Zhang, Z.; Yao, Z.; Li, Y.; Lu, S.; Wu, X.; Jiang, Z. Cation-induced $Ti_3C_2T_x$ MXene hydrogel for capacitive energy storage. *Chem. Eng. J.* **2022**, *433*, 134488.

(40) Patra, A.; Rout, C. S. Architecturally Robust $MoWS_2$ and $Ti_3C_2T_x$ MXene nanosheets hybrid for high performance energy storage and conversion applications. *J. Energy Storage* **2023**, *5*, No. e411.

(41) Zhan, X.; Si, C.; Zhou, J.; Sun, Z. MXene and MXene-based composites: synthesis, properties and environment-related applications. *Nanoscale Horiz.* **2020**, *5*, 235−258.

(42) Liu, L.; Laghari, A. A.; Meng, G.; Chen, H.; Wang, C.; Xue, Y. Photocatalytic disinfection of different airborne microorganisms by TiO_2/MXene filler: Inactivation efficiency, energy consumption and self-repair phenomenon. *J. Environ. Chem. Eng.* **2022**, *10*, 107641.

(43) Yang, J.; Cheng, S.; Zhang, S.; Han, W.; Jin, B. Modifying Ti_3C_2 MXene with NH_4^+ as an excellent anode material for improving the performance of microbial fuel cells. *Chemosphere* **2022**, *288*, 132502.

(44) Du, W.; Wang, F.; Fang, S.; Huang, W.; Cheng, X.; Cao, J.; Fang, F.; Wu, Y.; Luo, J. Antimicrobial PCMX facilitates the volatile fatty acids production during sludge anaerobic fermentation: Insights of the interactive principles, microbial metabolic profiles and adaptation mechanisms. *Chem. Eng. J.* **2022**, *446*, 137339.

(45) Zhang, Y.; Yun, S.; Wang, C.; Wang, Z.; Han, F.; Si, Y. Bio-based carbon-enhanced tungsten-based bimetal oxides as counter electrodes for dye-sensitized solar cells. *J. Power Sources* **2019**, *423*, 339−348.

(46) Jiang, Y.; Xie, X.; Chen, Y.; Liu, Y.; Yang, R.; Sui, G. Hierarchically structured cellulose aerogels with interconnected MXene networks and their enhanced microwave absorption properties. *J. Mater. Chem. C* **2018**, *6*, 8679−8687.

(47) Javed, M. S.; Zhang, X.; Ali, S.; Mateen, A.; Idrees, M.; Sajjad, M.; Batool, S.; Ahmad, A.; Imran, M.; Najam, T.; et al. Heterostructured bimetallic−sulfide@ layered $Ti_3C_2T_x$−MXene as a synergistic electrode to realize high-energy-density aqueous hybrid-supercapacitor. *Nano Energy* **2022**, *101*, 107624.

(48) Shakeel, S.; Khan, M. Z. Enhanced production and utilization of biosynthesized acetate using a packed-fluidized bed cathode based MES system. *J. Environ. Chem. Eng.* **2022**, *10*, 108067.

(49) Lim, K. R. G.; Shekhirev, M.; Wyatt, B. C.; Anasori, B.; Gogotsi, Y.; Seh, Z. W. Fundamentals of MXene synthesis. *Nat. Synth.* **2022**, *1*, 601−614.

(50) Numan, A.; Rafique, S.; Khalid, M.; Zaharin, H. A.; Radwan, A.; Mokri, N. A.; Ching, O. P.; Walvekar, R. Microwave-assisted rapid MAX phase etching and delamination: A paradigm shift in MXene synthesis. *Mater. Chem. Phys.* **2022**, *288*, 126429.

(51) Arshad, A.; Yun, S.; Si, Y.; Han, F.; Zhang, Y.; Zhang, Y.; Wang, Z.; Wang, C. Aloe vera-peel derived porous carbon integrated Co/Mn-oxide based nano-hybrids: An efficient electrocatalyst in advanced photovoltaics. *J. Power Sources* **2020**, *451*, 227731.